Accessible Full-Waveform LiDAR Data for Forest Monitoring

submitted by

Milto Miltiadou

for the degree of Doctor of Engineering

of the

University of Bath

Centre for Digital Entertainment

and of the

Plymouth Marine Laboratory

NERC Airborne Research Facility

November 2016

Abstract

no more than 300 words

NOTES:

Blue colour: additions according to Neill's feedback,

Red colour: notes

Gray colour: text that is going to be modified

To be added on top

Abstract

This study focuses on enhancing the visualisations and classifications of forested areas using coincident full-waveform (fw) LiDAR data and hyperspectral images. The ultimate aim is use both datasets to derive information about forests and show the results on a 3D virtual, interactive environment. Influenced by Persson et al (2005), voxelisation is an integral part of this research. The intensity profile of each full-waveform pulse is accumulated into a voxel array, building up a 3D density volume. The correlation between multiple pulses into a voxel representation produces a more accurate representation, which confers greater noise resistance and it further opens up possibilities of vertical interpretation of the data. The 3D density volume is then aligned with the hyperspectral images using a 2D grid similar to Warren et al (2014) and both datasets are used in visualisations and classifications.

Previous work in visualising fw LiDAR has used transparent objects and point clouds, while the output of this system is a coloured 3D-polygon representation, showing well-separated structures such as individual trees and greenhouses. The 3D density volume, generated from the fw LiDAR data, is polygonised using functional representation of object (FReps) and the marching cubes algorithm (Pasko and Savchenko, 1994) (Lorensen and Cline, 1987). Further, an optimisation algorithm is introduced that uses integral volumes (Crow, 1984) to speed up the process of polygonising the volume. This optimisation approach not only works on non-manifold object, but also a speed up of up to `51%` was achieved. The polygon representation is also textured by projecting the hyperspectral images into the mesh. In addition, the output is suitable for direct rendering with commodity 3D-accelerated hardware, allowing smooth visualisation.

In future work, the effects of combining both hyperspectral imagery and fw LiDAR in classifications and visualisations are examined. At first, two pixel wise classifiers, a support vector machine and a Bayesian probabilistic model, will be used for testing the effects of the combination in generating tree coverage maps. Higher accuracy classification results are expected when metrics from both datasets are used together. Regarding the visualisations, the differences of applying surface reconstruction versus direct volumetric rendering will be discussed and an ordered tree structure with integral sums of the node values will be used for speeding up the ray-tracing of direct volumetric rendering and improving memory management of aforementioned optimisation algorithm with integral volumes. Further, deferred rendering is suggested for testing the visual human perception of projecting multiple bands of the hyperspectral images on the FW LiDAR

polygon representations. At the end of this project the combination of the datasets will be used along with the watershed algorithm for tree segmentation, which is useful for measuring the stem density of a forest and for tree species classifications.

from EDE:

Firstly, a new and fast way of aligning the FW LiDAR with Remotely Sensed Images has been developed in DASOS and by generating tree coverage maps it was shown that the combination of those datasets confers better remote survey results. This work was presented at the 36th ISRSE International Conference.

Secondly, automated detection of dead trees in native Australian forests has a significant role in protecting animals, which live in those trees and are close to extinction. DASOS allow the generation of 3D signatures characterising dead trees. A comparison between the discrete and FW LiDAR is performed to demonstrate the increased survey accuracy obtained when the FW LiDAR are used.

Finally, the last application is for improving visualisations for foresters. Foresters have a great knowledge about forests and can derive a wealth of information directly from visualisations of the remotely sensed data. This reduces the travelling time and cost of getting into the forests. This research optimises visualisations by using the new FW LiDAR representations and a speed of up to 51% has been achieved.

FW LiDAR has great potentials in forestry and this research has already started to have an impact in the FW LiDAR community by making those huge datasets easier to handle. DASOS is now used at Interpine Group Ltd, a world leading Forestry Company in New Zealand and it has been tested from a PhD student at Bournemouth University who looks into estimating bird distribution in the New Forest. In the future, it is expected that DASOS will be widely used in remote forest surveys (i.e. estimating the commercial value of a forest and detecting infected trees at early stages for treatment).

Acknowledgements

Above all, I would like to express my great gratitude to my industrial supervisors Dr. Michael Grant who had supported me continuously during my research and gave me the freedom to create a project of my own interest.

Then, I would like to thanks Dr. Matthew Brown, who helped me during my first years of my studies by giving me valuable and informative feedback. He was always there to keep me working on the right track.

Equally important is my current supervisor Dr. Neil D.F. Campbell and he is not to be missed from the acknowledgements.

Furthermore, special thanks are given to Dr. Mark Warren, Dr. Darren Cosker, MSc Susana Gonzalez Aracil and Dr. Ross Hill who occasionally advised me during my studies.

It further worth giving credits to my data providers, the Natural Environment Research Council's Airborne Research Facility (NERC ARF) and Interpine Group Ltd.

Last but not least, I am extremely grateful to my funding organisations, the Centre for Digital Entertainement and Plymouth Marine Laboratory, who supported financially and consequently made this research possible.

Abbreviations and Glossary

AGC	Automatic Gain Controller
ALS	Airborne Laser Scanning
APL	Airborne Processing Library
ARF	Airborne Research Facility
DASOS	(=forest in Greek), the open source software implemented for managing FW LiDAR data
FW	Full-Waveform
GB	Gigabyte
LiDAR	Light Detection And Ranging
NASA	National Aeronautics and Space Administration
NERC	Natural Environment Research Council
TB	Terabyte
VLR	Variable Length Records
WPDF	Waveform Packet Descriptor Format
UK	United Kingdom

Publications

DASOS-User Guide, M. Miltiadou, N.D.F Campbell, M. Brown, S.C. Aracil, M.A. Warren, D. Clewley, D.Cosker, and M. Grant, Full-waveform LiDAR workshop at Interpine Group Ltd, Rotorua NZ, 2016

Alignment of Hyperspectral Imagery and Full-Waveform LiDAR data for visualisation and classification purposes, M. Miltiadou, M. A. Warren, M. Grant, and M. Brown, *The International Archives of Photogrammetry, Remote Sensing and Spatial Information Sciences*, vol. 40, no. 7, p. 1257, 2015.

Reconstruction of a 3D Polygon Representation from Full-Wavefrom LiDAR data, M. Miltiadou, M. Grant, M. Brown, M. Warren, and E. Carolan,*RSPSoc Annual Conference, New Sensors for a Changing World*, 2014.

Awards

EDE and Ravenscroft Prize - Finalist: Selected as one of the five finalists for this is a prestigious prize that recognises the work of best postgraduate researchers.

Student Poster Competition at Silvilaser.

Conference Presentations

ForestSAT Conference, Santiago, Chile, 2016 - Oral and Poster Presentation

Computer Graphics & Visual Computing (CGVC), Bournemouth, United Kingdom, 2016 - Poster Presentation

Silvilaser, La Grant Motte, France, 2015 - Poster Presentation

International Symposium of Remote Sensing of the Environment (ISRSE), 2015 - Oral Presentation

RSPSoc Conference, New Sensors for a Changing world, Aberystwyth, United Kingdom, 2014 - Oral Presentation

Contents

List of Figures

Chapter 1

Introduction

1.1 Forest Monitoring: Importance and Applications

Forest monitoring involves checking and observing the changes in the structure of the forests and their foliage over the years. It has a significant value in both sustainable and commercial forests, because it contributes into managing biodiversity, maintaining forest health and optimising wood trade procedures as explained below:

- **Biodiversity** plays a substantial role in ecosystem resilience [1] while various human activities affect biological communities by altering their composition and leading species to extinction [2]. For example, in Australian native forests many arboreal mammals and birds rely on hollow trees for shelters [3] . Hollow trees are trees that have hollows, which are semi-enclosed cavity on trunks and branches. They are formed by natural forces, like bacteria, fungi and insects and it takes hundreds of years to become suitable for animal/bird shelters. Unfortunately recent studies shown that there us likely to be a shortage of hollows available for colonisation in the near future [4] [5]. Therefore monitoring and protecting hollow trees have a positive impact in preserving biodiversity.

- **Forest Health**: Protecting vegetation from pests and diseases. An example of pests are the Brushtail Possums, which were initially brought to New Zealand for fur trade, but they have escaped and become a thread to native forests and vegetation [6]. In addition, anthropogenic factors have a negative impact to nature. For instance, acid rain is responsible for the freezing decease at red bruces because it reduces the membrane-associated calcium, which is important for tolerating cold [7]. Those changes in nature need to be monitor in order to preserve a healthy and resilience ecosystem.

- **Wood Trade**: Measuring stem volume and basal areas of trees contributes to forest planning and management [8]. For example, measuring stocking and wood quality would help into estimating the cost of harvesting the trees in relation to the stocking [9].

Traditionally, forest monitoring involves field work such as travelling into the area of interest and taking manual measurements. Regarding the need to monitor hollows, tree climbing with ladders and ropes gives very accurate results but it's dangerous, expensive, time consuming, and cannot easily scale into large forested areas [10] [11]. Therefore, automated ways of monitoring forests are essential and this is why Remote Sensing has a significantly positive impact in forestry.

1.2 Background Information about Remote Sensing and Airborne Laser Scanning Systems

Remote sensing refers to the acquisition of information about objects, for example vegetation and archaeological monuments, without physical contact and the interpretation of that information. The sensors used to capture the information are divided into passive and active. For example satellite photography is passive because information are collected from the reflected natural sun light, while Airborne Laser Scanners (ALS) are active because they emit laser beams and collects information from the backscattered laser energy [12].

According to Wanger et al, Airborne Laser Scanning (ALS) is a growing technology used in environmental research to collect information about the earth like vegetation and tree species. Comparing ALS with traditional photography, ALS is not influenced by light and it is therefore less dependant on weather conditions (ie. it collects information from below the clouds). The laser beam further penetrates the tree canopies allowing it to record information about the forest structure below the canopy, as well as the ground [13]. ALS methods are divided into pulse systems, which repeatedly emit pulses, and continuous wavelength systems that continuously emit light. They both acquire information from the backscattered laser intensity over time, but continuous wavelength systems are more complicated because they obtain one extra physical parameter, the frequency of the ranging signal. Further, according to Wehr and Lohr, continuous wavelength systems are 85 times less accurate than pulse systems [14].

LiDAR (Light Detection And Ranging) systems are passive and pulse laser scanning systems [14]. They are divided into two groups according to the diameter of the footprint left by the laser beam on the ground. This diameter depends on the beam divergence and the distance between the sensor and the target. The small-footprint

systems have a 0.2-3m diameter, have been widely commercialised and are mostly carried on planes (ALS systems). In contrast, the large-footprint systems have a wider diameter (10-70m) and during experiments they were mostly adjusted on satellites. Small-footprint systems record at higher resolution but it cannot guarantee that every pulse will reach the ground due to the small diameter of their footprint, making topographic measurements difficult. In contrast, large-footprint scanners have wider diameters and can therefore scan wider areas with the likelihood of recording the ground to be higher [15] .

In addition, there are two types of LiDAR data, the discrete and the full-waveform (FW). The discrete LiDAR records a few peaks of the reflected laser intensity, while the FW LiDAR stores the entire backscattered signal. The discrete LiDAR has been widely used and a 40% reduction of fieldwork has been achieved at Interpine Ltd Group, New Zealand, with that technology. Regarding the FW LiDAR, scientists understand their concepts and potentials but due to the shortage of available tools able to handle these large datasets, there are very few uses of FW LiDAR [16].

The design of the first FW LiDAR system was introduced in 1980s, but the first operational system was developed by NASA in 1999 [17]. The increased amount of information recorded within the FW LiDAR suggests many new possibilities and problems from the point of view of image understanding, remote surveying and visualisation. As an indication, a 9.3GB discrete LiDAR from New Forest, UK, corresponds to 55.7GB of FW LiDAR.

This research is focused on the representations of the FW LiDAR data and contributes in both forestry visualisations and classifications. Two datasets are used for testing and evaluation: the New Forest and the RedGum dataset. An in depth explanation of LiDAR systems and the specifications, differences and challenges of the two dataset are given in and Section 2. An overview of the thesis along with its aims, objectives and contributions are then outlined at Section 3.

Chapter 2

Acquire Data

The aim of this section is to give a practical and scientific insight into the acquisition of data, because a good knowledge of these methods and their limitations is essential for understanding the related research undertaken. The relations between the two main datasets used in this project are depicted on Figure 2-1 and briefly explained here:

- The **New Forest dataset** from the UK was provided by the Natural Environment Research Council's Airborne Research Facility (NERC ARF). Measurements were collected simultaneously a Leica ALS50-II LIDAR and AISA Eagle/Hawk hyperspectral radiometers on the 8th of April in 2010. It contains Discrete LiDAR, FW LiDAR and hyperspectral images.

- The **RedGum dataset** was acquired in Australia using a Trimble AX60 integrated LIDAR/Camera instrument over the time period from the 6th of March in 2015 until the 31st of March in 2015. It was provided by the RPS Australia East Pty Ltd. Only the FW LiDAR data are used here.

The ALS data are explained first, because they are the main focus of this research, and hyperspectral imagery is towards the end of the chapter. In Section 2.1, an in-depth description of ALS systems and the differences between discrete and FW LiDAR data is given. Section 2.2 briefly discusses the binary file format of the acquired LiDAR data and Section 2.3 is a discussion on the limitations, the differences and the advantages of two LiDAR instruments; the Leica and Trimble. The essential information about the hyperspectral imagery, which is only associated with the New Forest dataset, is then covered in Section 2.4.

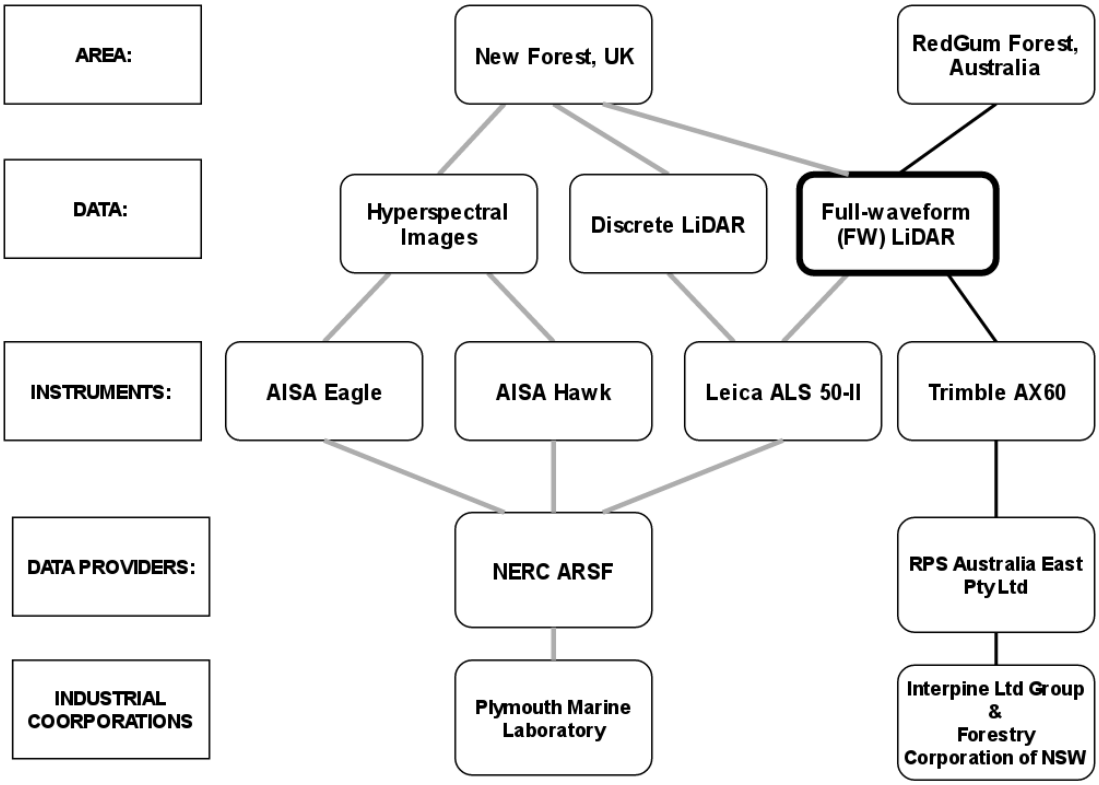

Figure 2-1: Data and Instruments

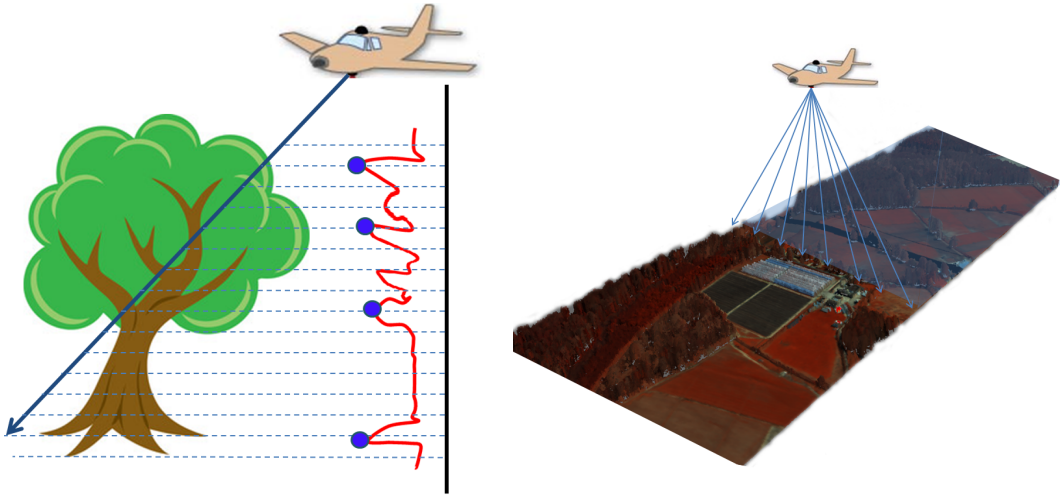

(a) A Pulse: Discrete Vs Full-Waveform (b) A Flightline

Figure 2-2: Airborne Laser Scanning System

2.1 Airborne LiDAR systems: An in-depth Explanation

The ALS systems emit laser pulses from sensor mounted in a plane and collects information from the time-of-flight and the returned laser intensity. By the time the pulse has travelled the approximately 1-3km from the aircraft to the ground, it is roughly 20cm in width due to beam divergence. When the pulse hits an object (i.e. the forest canopy), then some of it reflects back while the rest penetrates through holes between leaves and branches. The laser pulse continuous to hit structures, scattering and partially returning to the sensor until it reaches a solid barrier such as the ground and is fully blocked from further progress. The LiDAR systems record information from the backscattered laser pulse, measuring its round trip time and the returned intensity.

As mentioned at Section 1.2, there are two types of LiDAR data, the discrete and the FW. The discrete LiDAR observes the returned intensity signals and identifies and records a few peak points from the signal, while the FW LiDAR system digitises and records the enitre backscattered signal into equally spaced time intervals (Figure 2-2b). The delivered data for the discrete LiDAR is a set of hit points ("returns"), which are associated with laser intensities. The world position of every return is calculated by measuring the round trip time of the laser return, giving a distance from the sensor, which is combined with the precisely known position and orientation of the aircraft/sensor (from GPS, an inertial measurement unit and precise shot direction of the laser pulse). The waveform recordings are triggered by and attached to first returns of discrete LiDAR data (to avoid sampling the uninteresting time period while the pulse travels through the atmosphere) and they are a list of intensities that correspond to the laser intensity returned over time. There is also an offset vector which defines the distance and direction between each wave sample (effectively a compression mechanism, by avoid recording the world position of every sample, replacing it with the location of the first return and this vector).

As shown in Figure 2-2a, the pulses are scanned back and forth across the landscape below (by a rotating mirror) as the plane travels forward. The scanned data has a limited maximum width according to the flight height and the field of view scan angle. During processing the track of the plane is divided into easier-to-handle pieces (flightlines) and saved into separate binary files. In this project the LAS1.3 file format is used for both datasets.

2.2 Brief Description of the LAS1.3 File Format

There are a few LiDAR file formats but the LAS1.3 was the first format to contain FW data and it is the one used to store the data for both New Forest and RedGum datasets. According to the LAS1.3 file specifications [18], a .LAS file contains information about both discrete and FW LiDAR data, with the waveform packets are attached to discrete returns and saved either internally at the end of the .LAS file or externally in a .WVS file.

As shown at (Figure 2-3) the .LAS file is divided into four sections and a brief explanation of each section is given here:

1. The **Header** contains general information about the entire flightline. For example, it includes the maximum scan angle used during the flight, whether the waveform packets are recorded internally or externally and the number of **Variable Length Records** (VLR).

2. Regarding the **VLR**, which contain arbitrary "extension" data blocks, the most important information given is the waveform packet descriptors that contain essential information on how to read the waveform packets (i.e. an ID, the number of wave samples and the size of each intensity in bits).

3. The **Point Data Records** are the discrete points and the waveforms are associated with first return discrete points. Each Point Data Record has a spatial location, an intensity and optionally a pointer to a waveform packet as well as the ID of the corresponding waveform packet descriptor.

4. The waveform packets is a list of intensities and they are either saved internally into the **Extended Variable Length Records** section of the .LAS file or inside an external .WVS file. Starting from the associated first return point, the spatial locations of the waveform packet (wave sample intensity) are calculated by adding an offset defined in the associated Point Data Record.

2.3 Leica Vs Trimble Instruments: Limitations, Differences and Advantages

As shown in Figure 2-1, the Leica ALS 50-II instrument was used to capture the LiDAR data of New Forest dataset and the Trimble AX60 for collecting the RedGum Forest FW LiDAR data. It is therefore important to clarify the differences, the limitations and the advantages of each instrument.

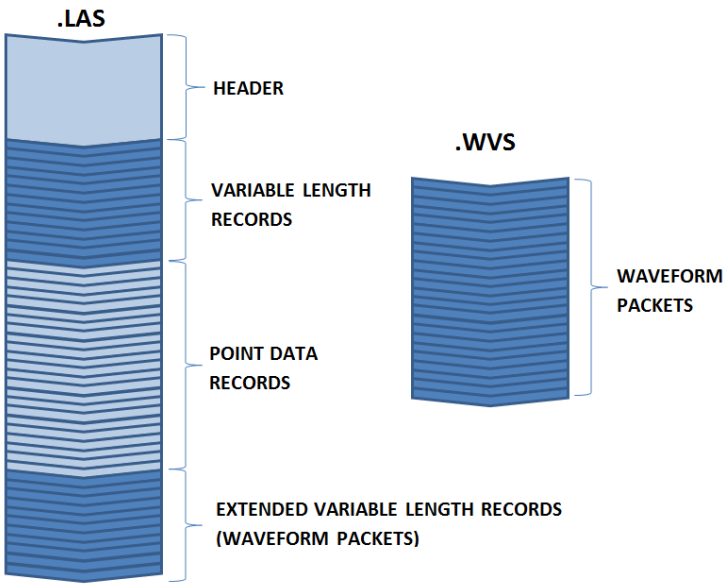

Figure 2-3

The Trimble performs at a pulse frequency of 400kHz, while the Leica's maximum pulse frequency is 120kHz. Nevertheless, during experiments there were occasions when the Leica discarded every other waveform due to I/O limitations despite being at or below the maximum pulse frequency [19]. The New Forest dataset has been affected by this and, on average, one third of the saved pulses only contain discrete data. We should therefore be extremely careful when comparing Discrete with FW LiDAR data. While [16] concludes that FW LiDAR data worth the extra processing because they have a better vertical profile, [20] states that extra information (the echo-width) from the FW LiDAR data are relatively unimportant. But the New Forest datasets were used for the comparison at [20] and there is no mention about the significantly less waveforms recorded in comparison to the discrete data. It is therefore suspected that their results has been affected by the missing waveforms.

Another problem with the Leica sysyem is the small dynamic range of intensities due to the number of bits used for recording them; the Leica system uses 8-bit integers (0-255 range) while the Trimble uses 2-bit integers (0-16385 range). For increased dynamic range and finer intensities without doubling storage costs, Leica introduced an Automatic Gain Controller (AGC). The AGC is an 8-bit number that defines how the recorded intensity range is shifted across a wider range of intensities. The AGC value is adjusted according to the reflected laser intensity of the previous 64 pulses and it therefore varies across a flightline. Consequently, the raw intensities are incomparable to each other and, since the relation between AGC and the intensities is not linear,

the range normalisation is complicated [21] [22]. In this thesis, the intensities of the Leica system are used as boolean values (whether something existed or not, using a user-defined threshold) to quickly overcome that issue and focus on the major research objectives. Regarding the Trimble instrument, there is no AGC value because the intensities are saved into a 16bit integer and as long as the flight height is constant no normalisation is required. In a few words, the raw intensities recorded using the Leica system are not normalised and therefore not comparable to each other, while the intensities of the Trimble instrument are more meaningful.

The footprint of the laser on the ground depends on the scanning pattern of the instruments and the field of view. The sinusoidal scanning pattern of the Leica system results in a higher density of returns at the edges of the flightline. The footprint of the Trimble instrument is more equally spaced because they are scanned using a rotating polygon. The uneven density pattern of the Leica system is resolved by normalisation during the voxelisation process, but the Trimble's equally spaced pulse pattern is more prone to aliasing when voxelised. Regarding the field of view, the Leica is wider but both systems avoid large angles because otherwise data look deformed at edges of the flightlines.

Last but not least, the Trimble instrument is a native full-waveform sensor; the discrete LiDAR are produced by extracting peak points in post-processing. Therefore one of the purported advantages of a FW system, the concept of extracting a denser point clouds using Gaussian decomposition [13], does not apply in the Trimble's case. This was proven by extracting peak points from Trimble FW LiDAR data using the pulseextract from LAStools [23]; the number of points extracted was exactly the same as the number of points saved into the associated discrete LiDAR files. Therefore discrete data from the Trimble instrument are the same as those generated by echo decomposition and peak points extraction from the FW samples.

To sum up, the Trimble AX60 instrument is a newer sensor and therefore has less problems or design compromises in comparison to the Leica ALS50-II instrument. Table **??** summarises the differences between the two sensors.

2.4 Hyperspectral Imagery

Hyperspectral imagery has a positive impact in remote sensing because it contains information beyond human visibility. The human eye receives light from the visual spectrum into three bands (red, green and blue). The hyperspectral sensors captures a larger spectrum and divides its light components into hundreds of bands, recording this way more information than a human eye can receive [12].

Instrument Name:	**Leica ALS550-II**	**Trimble Ax60**
Scanned Area	New Forest, UK	RedGum, Australia
Year of Introduction:	Discrete LiDAR 2009 & FW LiDAR 2010	2013
Max Scan Frequency (kHz):	120	400
Recorded Intensity (bits):	8	16
AGC:	Yes	No
Scanning Pattern:	Sinusoidal	The footprints are more equally spaced on the ground
Max field of view (degrees):	75	60

Table 2.1: Specifications of the LiDAR instruments used

Nevertheless, there are other compromises - for example, the time taken to integrate incoming light as the aircraft carrying the sensors moves. This means the raw airborne images appear deformed because the pixel length varies across the flightline. NERC-ARF geo-corrects the data using the Airborne Processing Library (APL) [24]. The processing levels are numbered. At 'level 3' (world coordinate system) the pixels are equally spaced and sized, which requires resampling and thus may look slightly blurred. The 'level 1' data (what the sensor saw) are non geo-corrected but they are associated with a file that defines the spatial location of each pixel. In this thesis, the 'level 1' data are used to preserve the highest possible quality.

In practise, the level 1 data are held in two files, the '.bil' and the '.igm'. The '.bil' file contains the hyperpsectral cube (Figure 2-4), all the pixel values at different wavelengths, and the .igm file gives the x, y, z coordinates of each pixel.

The number of bands and the spectrum range captured depends on the hyperspectral sensor. The data from New Forest were collected using the following instruments:

- the Eagle, which captures the visible and near infra-red spectrum (400-970nm)
- the Hawk, which covers short wave infra-red wavelengths (970-2450nm)

Both sensors divide their spectral range into 252 bands (programmable) and each band is a 2D vector as shown in Figure 2-4).

The hyperspectral images also come with a number of drawbacks. A few are mentioned here but since hyperpsectral imagery is not the main focused of the thesis there are not addressed:

- System faults sometimes occurs and the affected areas are masked out. This results in blank areas.

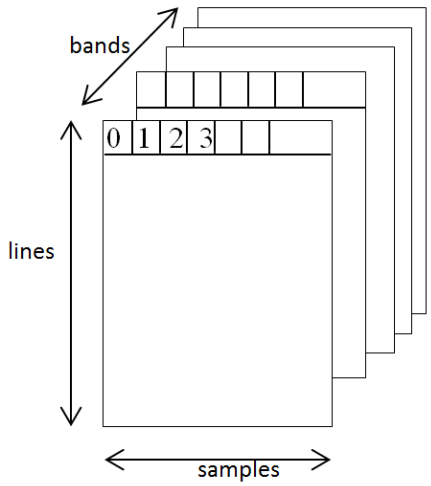

Figure 2-4: This figure shows the order of the hyperspectral pixels saved into the the binary .bil file.

- As a passive sensor, it is dependent on the sun for illumination and thus vulnerable to poor weather conditions
- Due to the high refraction of light at some wavelengths, some bands are highly influenced by humidity (i.e. wavelength 1898.33).

To sum up, hyperpsectral images contain information beyond the visible and they are delivered in two files, one contains the hyperspectral cube and the other one the geo-locations of each pixel. In this project, they are used in chapter (Chapter 7), where it is shown that the combination of Remote Sensing data confers better results for generating tree coverage maps.

Chapter 3

Overview of Thesis

3.1 Problem

FW LiDAR systems have been available for a number of years but there still very few uses of FW LiDAR data. NERC-ARF has been acquiring airborne data for the UK and overseas since 2010 and it has more than 100 clients of new and archived data. Many clients request FW LiDAR data to be acquired, but despite the significant number of requests, the discrete LiDAR data has been mostly used on research instead. Some of the factors regarding this slow intakes are:

- Typically FW datasets are 5 – 10 times larger than discrete data, with data sizes in the range of 50GB – 2.5TB GB for a single area of interest. NERC-ARF's datasets are up to 100GB each because most clients are research institutes but for commercial purposes each FW dataset is a couple of TB.
- Existing workflows are only able to work with the discrete data since the increased amount of information recorded within the FW LiDAR makes handling the quantity of data very challenging.

3.2 Aims and Objectives

This thesis explores visualisation and data-understanding for FW LIDAR systems and the overarching aim is to increase the accessibility FW LiDAR in remote forest surveying.

The objectives are the following:

- Enable forestry experts with no computer science expertise to visualise and work with the FW LiDAR data.

- Enable understanding of the FW LiDAR data through 3D visualisations.
- Improve and optimise visualisations of full-waveform LiDAR data and hyperspectral images.
- Enable browsing of very large scale datasets and spectral bands in an efficient manner.
- Investigate data structures for faster iso-surface extraction of large volumetric datasets and efficient management of voxels.
- Estimate tree coverage and investigate the potential of integrating multiple remote sensing datasets in forestry.
- Dead tree detection in comparison to human detection and remote surveying with discrete LiDAR that will benefits biodiversity management.
- Research whether terrain classification can be improved by the inference of high quality 3D information, for example, using priors over the space of 3D elements.

3.3 Overview

*** the following text has been taken from the IAA2 funding application

To address the limitations of existing workflows for using with FW data we developed the open source software DASOS ($\delta\alpha\sigma o\varsigma$=forest in Greek) and novel algorithms that allow users, without computer science expertise, to work with and visualise large volumes of FW LiDAR data. Our open source software DASOS aims to remove the barriers preventing the use of FW LiDAR. Its contributions, and those of the new representations of the FW LiDAR, are demonstrated in three applications:

- Firstly, foresters can exploit their domain expertise to derive a wealth of information by observing the FW LiDAR data. We therefore improve visualisations for deriving information directly from the data, thus reducing travelling time and the associated expenses of getting into the forests. This cost includes appropriate cars and sometimes helicopters depending on the accessibility of the forests. While previous work on FW LiDAR visualisation talks about point cloud visualisation [25] and transparent voxels [26], DASOS is able to reconstruct the surfaces from the scanned area in 3D. This research further optimisesvisualisations by using the new FW LiDAR representations to accelerate this process by up to****% so far.

- Secondly, a fast way of aligning the FW LiDAR with Remotely Sensed Images has been developed in DASOS. Subsequently, by generating tree coverage maps, it has been shown that the combination of these datasets confers better remote survey results [27].

- Finally, DASOS allow the generation of 3D priors. An example usage of this information is characterising dead standing Eucalyptuses, which as explained at Section ?? are extremely beneficial for managing biodiversity in native Australian forests. This is work in progress and a comparison between the discrete and FW LiDAR will be performed to demonstrate the increased survey accuracy obtained when the FW LiDAR is used.

In summary, FW LiDAR has great potential to improving automated surveying accuracy and consequently reduce the expensive fieldwork conducted in forestry and this research has already started to have an impact in the FW LiDAR community. DASOS is now used at Interpine Group Ltd, a world leading Forestry Company in New Zealand, and a PhD student at Bournemouth University is evaluating it for use in the estimation of bird distributions in the New Forest in the UK.

*** end of copied text

3.4 Structure

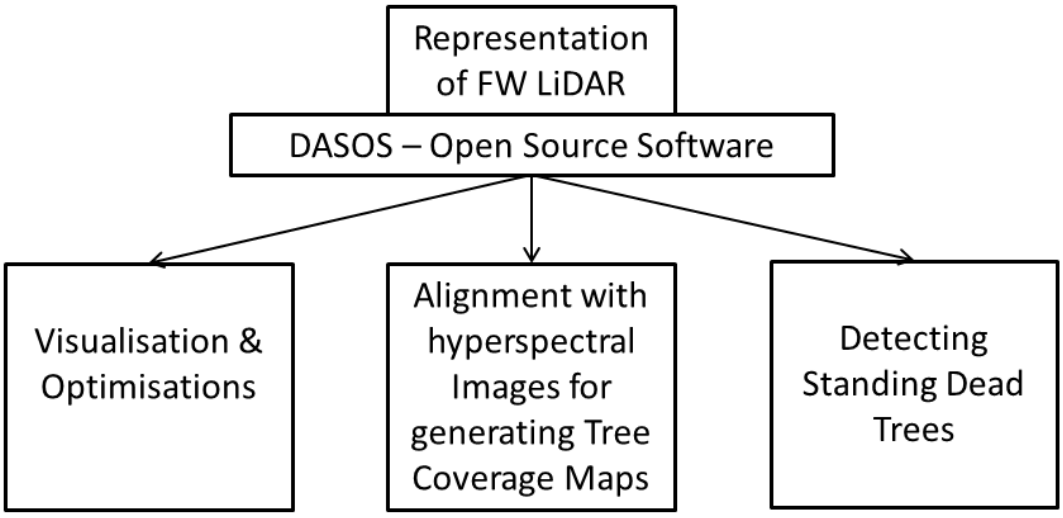

Figure 3-1: The pipeline of the thesis

Chapter 4

DASOS

DASOS can produce 3D polygons and metrics useful in deriving information about the scanned areas

Chapter 5

Voxelisation

5.1 Background Information

*** Neill: the following paragraphs were moved here from the Background Chapter 1.2

The most common approach of interpreting the FW LiDAR is the Gaussian decomposition of the waveforms and extraction of peak points [28]. Neunschwander et al used this approach for Landcover classification [29] while Reitberger et al applied it for distinguishing deciduous trees from coniferous trees [30]. Chauve et al further proposed an approach of improving the Gaussian model in order to increase the density of the points extracted from the data and consequently improve point based classifications of FW LiDAR data [17].

While echo decomposition identifies significant features as points, the FW LiDAR data also contains information in single shots that may be below the significance threshold. The waveform samples data can be accumulated from multiple shots into into a voxel array, building up a 3D density volume. The correlation between multiple pulses into a voxel representation produces a more accurate and complete representation, which confers greater noise resistance and it further opens up possibilities of vertical interpretation of the data. Voxelisation of FW LiDAR data was firstly introduced by Persson et al, who used it to visualise the waveforms using different transparencies [26] and it seems to be the future of FW LiDAR data with the literature moving toward that direction. In 2016, Cao et al used it for tree species identification [31] and Sunmall et al characterised forest canopy from a voxelised vertical profile [20]. This innovative approach is an integral part of this thesis and it is used for both visualisations and classifications [32] [27].

*** end of moved paragraphs ***

5.2 Approach

The FW LiDAR data are voxelised by inserting the wave samples into a 3D regular grid and constructing a 3D discrete density volume. According to Person et al, each wave sample is associated with the 3D cell, named voxel, that it lies inside. If multiple samples lie inside a voxel then the sample with the highest intensity is chosen [26]. In order to reduce noise, there are two differences between this approach and the way FW LiDAR data are voxelised in DASOS.

At first a threshold is used to remove low level noise, because when the width of a recorded waveform is longer that the distance between the first hit point and the ground, the system captures low signals, which are pure noise. For that reason, the samples whose intensity is lower than a user-defined noise level/threshold are discarded.

Then each wave sample is associated with the voxel that it lies inside and the second difference is how DASOS overcomes the uneven number of samples per voxels. The intensity of each sample is the laser intensity returned during the corresponding time interval. For example, if 5 samples are inside a voxel and the waveform is digitised at 2ns, then the laser intensity associated with that voxel corresponds to 10ns waveform width. For comparison purposes, it's essential to keep the waveform width consistent across the voxels. For overcoming this issue in DASOS, the average intensity of the samples that lie inside each voxel is taken, instead of choosing the one with the highest intensity [26]. This way the likelihood of the 3D volume to be affected by outliers and high noise is reduced. The following equation shows how the intensity value of a voxel is calculated:

$$I_v = \frac{\sum_{i=1}^{n} I_i}{n} \tag{5.1}$$

where I_v is the accumulated intensity of voxel v. n is number of samples associated with that voxel, I_i is the intensity of the sample i,

To sum up, during voxelisation the area of interest is divided into voxels. The samples of the FW LiDAR data are inserted inside this 3D discrete density volume and normalised such that equally sized waveform width is saved inside each voxel. The result is a 3D discrete density volume of the scanned area. Figure 5-1 depicts this process in 2D.

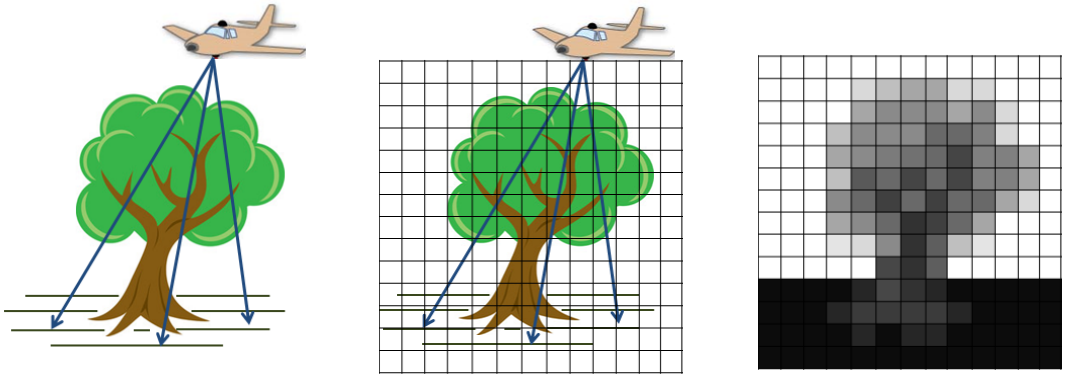

(a) The sensor from the plane emits multiple pulses and collects information from the returned laser intensity.

(b) The area of interest is divided into equally sized cubes, named voxels, generating this way a discrete volume.

(c) The accumulated intensities of wave samples into the volume build up the voxelised representation of the scanned area.

Figure 5-1: The above images depict the voxelisation process of the FW LiDAR data in 2D. Please note that the voxelisation output in Figure 5-1c shows how ideally the result would look. But in reality, a number of trees may be disconnected from the ground due to missing information about their trunk.

5.3 Implicit Representation of the Volume

Implicit objects were introduced by Blinn in 1982 [33] and enable the definition of complex objects without saving a large amount of triangles. Each one is defined by a function $f(X)$ and the iso-surface value α. The iso-surface value defines the boundaries of the object; for an object $[f(x), a]$ every n-dimensional point X that lies on the surface of the object satisfies the condition $f(X) = \alpha$. To be more specific, all the following rules apply according to Pasko et al [34]:

- f(X) $= \alpha$, when X lies on the surface of the implicit object
- f(X) $> \alpha$, when X lies inside the implicit object and
- f(X) $< \alpha$, when X lies outside the implicit object

Once the discrete density volume is generated, an implicit object is defined to represent the scanned area.

Regarding the implicit representation of the 3D voxelised FW LiDAR data, X is a three dimensional point (x, y, z) representing the longitude, latitude and height respectively and $f(X)$ is a function that takes X as input and returns the accumulated intensity value of the voxel that X lies inside. Also, the iso-surface value α is a user

defined parameter and it is noise dependant (Please look at figure *** to understand how the iso-surface value affects the implicit representation of voxelised FW LiDAR data).

5.4 Summary

This thesis strongly supports voxelisation of FW LiDAR data. Voxelisation preserves an extra parameters in comparison to point extraction algorithms, the pulse width [20]. It also accumulates intensity values from multiple shots and stores them into a 3D regular grid, resolving this way the sinusoidal footprints pattern of the Leica system; all the voxel values are normalised and contain an intensity value that corresponds to equal waveform width. Voxelisation is further supported by the recent literature [31] [20].

In a few words, the FW LiDAR data are voxelised by inserting the wave samples into a 3D discrete density volume. Then an implicit representation of that volume is defined by the function $f(X)$ and the iso-surface value α. The function $f(X)$ takes as input a point X and returns the associated intensity of the voxel that X lies inside. If the returned intensity is greater than the value α then X lies inside the implicit object, if it is is equal to α then it is on the boundary otherwise it lies outside.

Chapter 6

Visualisations

This chapter focuses on the visualisations of voxelised FW LiDAR data and their management in memory.

*** Previous Work ***

So far, the concepts of FW LiDAR data (Section 2) and voxelisation (Section 5) has been explained, as well as how the implicit object $[f(X), \alpha]$ is represented. This sections explains how the data are visualised in 3D, as well as the new data structures implemented and introduced for speeding up the surface reconstruction process.

6.1 Surface Reconstruction

Even though numerical implicitisation is beneficial in reducing storage memory and for various resolution renderings of the same object, visualising numerical/algebraic objects is not straight forward, since they contain no discrete values. This problem can either be address either by ray-tracing or polygonisation. In 1983, Hanraham suggested a ray-tracing approach, where an equation is derived from the ray and surface intersection [35].

The Marching Cubes algorithm was later introduced for polygonising implicit objects, using a look up table. Let's assume that $f(X)$ defines an implicit object. At first the space is divided into cubes. Each cube is defined by eight corner points, which lie either inside or outside the object. By enumerating all the possible cases and linearly interpolating the intersections along the edges, the surface of the implicit object is constructed [36]. According to Lorensen and Cline, the normal of each vertex is calculated by measuring the gradient change. But in this case, due to the high gradient changes inside the volume, this approach of calculating the normal leads to a non-smooth visualisation. For that reason, the normal of each vertex is derived by the average of its adjacent triangles.

Further the sampling of the Marching cubes is independent from the sampling of the 3D density volume, but consistency between the two is required. Let's assume the discrete volume has (n * m * k) voxels. The volume can be sampled into cubes at any rate but to reduce aliasing a ((n+1) *(m+1) * (k+1)) dimensional sampling is suggested. Please note that every point that lies outside the volume is considered to be below the boundary threshold and set to a value lower than the isosurface value. An example of the corresponding sampling in 2D is shown on Figure 1, where the black grid represents a 2D density table and the blue grid represents the sampling used in during polygonisation.

The following table shows the effects of oversampling during polygonisation. The right image was oversampled and the second one was sampled as explained above.

6.1.1 Results

modifying iso-surface, noise level, & selecting region of interest & various flightlines

6.2 Optimising Surface Reconstruction

The original Marching Cubes algorithm uses a scan line approach and processes all the cubes sequentially. The scan line approach sometimes implies looping through large amounts of empty cubes. To optimise the process, in this research, it is proposed an algorithm that repeatedly divides the volume and utilities Integral Volumes to discard empty volumes during the polygonisation. Using this optimisation algorithm it was achieved an up to 51This optimisation algorithm is explained in the following sections, which are structured as follow: - Background information, including previous related work. - How integral images are extended into 3D. - The proposed algorithm of using Integral Volumes to speed up the process of polygonising an implicit object using the Marching Cubes algorithm - Implementation details that contribute to the efficiency and speed up of the algorithm - Results

6.2.1 Background

Much research has been done so far on optimising and improving the polygonisation of implicit surfaces. But most research is based on closed and manifold object. A polygon mesh is closed when it has no holes and it is manifold when it can be unfolded into a 2D continues surface. In order to guarantee consistent topology, an optimised approach with an enhanced look up table was proposed by Lewiner et al in 2003.

Further surface-tracking was discussed in both papers of (Rodrigues de Araujo and Pires Jorge, 2005) (Hartmann, 1998). Starting from a seed point, the surface is expanded according to the local curvature of the implicit object. Self-intersections and collisions are avoided using heuristic edge length. This method is considered to be faster and more efficient, in comparison with the Marching Cubes algorithm. Because, by tracking the surface, huge empty spaces are not searched and it is also possible to create smaller triangles on places with high gradient changes and bigger triangles on surfaces with low variance. Nevertheless, surface-tracking Algorithms cannot be applied in our case though, because the output of on my program is a non-manifold objects. The 3D Volume generated from FW LiDAR data is not consistent, since small footprint Leica FW systems cannot guarantee that the last return is from the ground. For that reason, it is possible that some trees may be separated from the ground. Surface-tracking algorithms converge once the object is closed. Therefore, there is a possibility that they may converge after polygonising a single tree if the seed point lies on a tree that is separated from the ground.

In 1992, Hansen and Hinker proposed parallelising the polygonisation process of BlobTree trees on Single Instruction, Multiple Data (SIMD) machines. BlobTree trees represent implicit objects as a combination of primitives and operations likes union and blends (Galbraith, MacMurchy, and Wyvill, 2004). While the depth of the tree increases, the time required to get the value that defines whether a point is inside or outside the object increases as well. On SIMD machines greater speed up is achieved at longer instruction due to the less communication cost. Therefore parallelising the process of BlobTree trees with long depth is beneficial, but in our case the value returned for a given point is calculated in constant time. Further, according to the C++ Coding Standards by Sutter and Alexandrescu, when optimisation is required is better to seek an algorithmic approach first because it is simpler to maintain and the possibility of being bug free is higher (Sutter and Alexandrescu, 2004).

OpenVDB library manages volumetric data with octrees. My program uses 1D arrays allowing constant time access of voxel values and by importing OpenVDB library, its speed was significantly decreased; while the number of voxels is increasing the time required to get the value of a voxel is also increasing. Further according to the documentation, the VolumeToMesh class “meshes any scalar grid that has a continuous isosurface”, while the surface of the FW LiDAR volumes is not continuous; there are triangles that represent leafs inside the trees and some of the trees may be disconnected from the ground because the last return do not always reach the earth (OpenVDB 2.3.0).

In this report, it is introduced a new method of optimising the marching cubes algorithm. This method utilises Integral Volumes (an extension of Integral Images) to discard chunks of empty cubes during polygonisation. Its effectiveness stands at the ability of integral volumes to find the sum of any sub-volume into constant time and it is important because it works effectively non-manifold or non-closed objects.

6.3 Integral Volumes

In 1984, Crow proposed an image representation where each pixel value is replaced by the sum of all the pixels that belong to the rectangle defined by the lower left corner of the image and the pixel of our interest (Crow, 1984). Even though more storage space is required to save the image, due to the larger numbers, the sum of every rectangle in the image can be calculated in constant time, once the table is constructed. The integral image can also be constructed in linear time O(n), where n is the number of pixels in the image. One iteration through the entire image is enough to replace the pixel values of the image.

image

Chapter 7

Alignment with Hyperspectral Imagery

7.1 Previous Work

Regarding the integration of FW LiDAR and hyperspectral in remote forest surveys, Clark et al attempted to estimate forest biomass but no better results were observed after the integration [37]. While the outcomes of Aderson et al for observing tree species abundances structures were improved after the integration of data [38].

[39] Buddenbaum et al, 2013, and [40] Heinzel and Koch, 2012, used a combination of multi-sensor data for tree classifications. Buddenbaum et al use fusion of data to generate RGB images from a combination of FW LiDAR and hyperspectral features, although the fusion limits the dimensionality of a classifier [39]. Further, in their study, three different classifiers were implemented and the Support Vector Machines (SVMs) returns the best results. SVMs were also used in [40] to handle the high dimensionality of the metrics (464 metrics). In that research a combination of FW LiDAR, discrete LiDAR, hyperspectral and colour infrared (CIR) images are used. Each of the 125 hyperspectral bands is directly used as a feature in the classifier, contributing to the high dimensionality. Here, some of the FW LiDAR and LiDAR features are used but in a digested form (i.e. the width of the waveform), and matches to the spectral signatures of each class are used to reduce the dimensionality.

7.2 Visualisation

To enhance the visualisation of FW LiDAR data, a volumetric approach of polygonising the data was proposed by Miltiadou et al, 2014. First, the waveforms are inserted into

a 3D discrete density volume, an implicit object is defined from the volume and the object is polygonised using the Marching Cubes algorithm. In this paper we emphasis the sampling of the volume versus the sampling of the Marching Cubes algorithm as well as the effects of using full-waveform versus discrete LiDAR. Further hyperspectral imagery is introduced to improve the visual output and allow parallel interpretation of the data.

7.3 Integrating hyperspectral Imagery

When the hyperspectral images are loaded along with the LiDAR files, then the outputs are:

1. the 3D geometry, which contains all the information about the vertices, edges, faces, normal and texture coordinates, and

2. a texture, which is an RGB image which is aligned with the texture coordinates of the polygon mesh.

For every scanned area, there are both FW LiDAR and hyperspectral data, but since the data are collected from different instruments they are not aligned. To integrate the data geospatially, aligning the data is required. In order to preserve the highest possible quality and avoid blurring that occurs during georectification, data in original sense of geometry (level 1) are used.

Here it worth mentioning that the texture coordinates (u, v) of each vertex lies in the range [0, 1] and if they are multiplied by the height/width of the texture, then the position of the corresponding pixel of the 2D texture is given. The 2D texture is simply an image generated from three user-selected bands for the RGB colours and its width is equal to the number of samples per line while its height is equal to the number of lines.

(***doesn't apply anymore) Further the values of the three user-defined bands are normalised to lie in the range [0,255].

DASOS projects level 1 hyperspectral images by adjusting the texture coordinates of the polygon according to the geolocation of the samples. That is, for each vertex (xv, yv , zv) we find the pixel, whose geolocation (xg, yg) is closest to it. Then by using the position of the pixel on the image (xp, yp), the texture coordinates of the vertex are calculated accordingly.

For speed up purposes, we first import the pixels into a 2D grid, similar to Warren et al, 2014. The dimensions of the grid and the length of squares are constant, but

in our case the average number of pixels per square (Aps) can be modified and the dimensions (nx, ny) of the grid are calculated as follow:

**** EQUATION *****

where ns = the number of samples and nl = the number of lines in the hyperspectral images.

Furthermore, while Warren et al use a tree-like structure, here structure similar to hash tables is used to speed up searching. Hash table is a data structure, which maps keys to values. In our case, we utilise the unordered_multimap of c++11 (a version of the c++ programming language), where for every key there is a bucket with multiple values stored inside. Each square (xs,ys) has a unique key, which is equal to (xs + ys *nXs) and each pixel is associated with the square it lies inside. In other words, every key with its bucket corresponds to a single square of the grid and every bucket includes all the pixels that lie inside that square. The next step is for every vertex (xv, yv, zv) to find the pixel whose geolocation is closest it. First we project each vertex into 2D by dropping the z coordinate and then we find the square (xs , ys) that its projection (xv , yv) lies in, as follow:

**** EQUATION *****

**** EQUATION *****

where maxX, minX, maxY, minY = the geolocation boundaries of all the hyperspectral image.

From the square (xs,ys) we can get the set of pixels that lie inside the same square with the vertex of our interest. Let's assume that the positions and geolocations of these pixels are defined by p1 , p2 , p3, ... , pn and g1, g2 g3 , ... , gn respectively. Then, by looping through only that set of pixels, we can find the pixel i that lies closest to the vertex v(xv , yv)

**** EQUATION *****

Finally, we need to scale the pixel position pi = (xp, yp), such that it lies in the range [0,1]. The scale factors are the number of samples (ns) and lines (nl) of the hyperspectral image. So, the texture coordinates (u, v) of each vertex v(xv , yv) are given by the following:

**** EQUATION *****

Chapter 8

Classifications

This talk presents the new features of DASOS, which is an open source software for managing full-waveform LiDAR data and those features are used for detecting dead standing Eucalypt.

The value of dead standing Eucalypt trees from a biodiversity management perspective is large. In Australia, many arboreal mammals and birds that are close to extinct inhabit hollows [5]. Nevertheless, studies predict shortage of hollows in the near future due to tree harvesting and the decades required for a tree to be mature enough to develop a hollow [3] [4]. Dead standing eucalypt trees are more likely to be aged and have hollows, therefore automated detection of them plays a significant role in protecting animals that rely on hollows.

DASOS (= $\delta\acute{\alpha}\sigma o\varsigma$) means forest in Greek and it is an open source software aiming to ease the way of handling FW LiDAR data in forestry [27]. Traditional ways of interpreting FW LiDAR data, suggests extraction of a denser points cloud using Gaussian decomposition [29] [30]. Nevertheless DASOS was influenced by Persson et al, 2005, who used voxelisation to visualise the waveforms [26]. But, DASOS do not only uses voxelisation for visualisations but also for extracting metrics useful in classification. It further normalises the intensities so that equal pulse length exists inside each voxel, making intensities more meaningful. It is further seems that the literature is moving towards voxelisation with the good results obtained at recent publication on tree species classification [31].

The new features of DASOS: New features of DASOS which enables observation at tree level: i.e. distribution of intensities at specific area

The data, provided by RPS Australia East Pty Ltd, were collected in March 2015 from the Riegl (LMS-Q780 or LMS-Q680i?) sensor at an Australian native Forest with eucalyptus. The fieldplots has been provided by (Interprine Group Ltd or Forest

Corporation?).

examined with Random Forest

The new features of DASOS are presented and used for generating 3D signatures characterising dead standing trees and a comparison between the discrete and FW LiDAR data is performed to demonstrate the increased survey accuracy obtained with the FW LiDAR.

This paper presents a new feature of DASOS, which is an open source software for managing full-waveform (FW) LiDAR data and that feature is used for detecting dead standing Eucalypt trees in native Australian forests.

The value of dead standing Eucalypt trees from a biodiversity management perspective is large. In Australia, many arboreal mammals and birds, which are close to extinct, inhabit hollows [5]. Nevertheless, studies predict shortage of hollows in the near future due to tree harvesting and the decades required for a tree to develop a hollow [3] [4]. Dead standing eucalypt trees are more likely to be aged and have hollows, therefore automated detection of them plays a significant role in protecting animals that rely on hollows.

The LiDAR data used for this project are provided by RPS Australia East Pty Ltd and they were collected in March 2015 using the Riegl (LMS-Q780 or LMS-Q680i?) sensor. The Riegl LMS-Q??? is a native full-waveform sensor and the LiDAR point clouds were generated from the waveform instrument data during post processing. In addition, the field plots used for the classifications are provided by (Interprine Group Ltd or Forest Corporation?) and contain around 1000 Eucalypt trees while 10% of them are dead.

The new feature of DASOS calculates forestry metrics within a radius relevant to canopy height and exports all metrics into a single vector for fast interpretation in advanced statistical tools. Traditional ways of interpreting FW LiDAR data, suggests extraction of a denser points cloud [29] [30], but as mentioned before with the Riegl system this is done at post processing. Nevertheless DASOS was influenced by Persson et al, 2005, who used voxelisation to visualise the waveforms [26], but DASOS also uses it for generating metrics. It further normalises the intensities so that equal pulse length exists inside each voxel, making intensities more meaningful. Further, recent publication on tree species classification showed that voxelisation could confer good results while interpreting FW LiDAR data [31].

Previous work on dead standing trees detection, suggests single tree segmentation before dead trees identification [41] [42] but in case of Eucalypt trees single tree detection is a challenge on its own due to their irregular structure and multiple trunk splits.

In this project, the new feature of DASOS is used for generating 3D signatures characterising dead standing Eucalypt trees and a comparison between the LiDAR point cloud and FW LiDAR data is performed using Random Forest to demonstrate the increased survey accuracy obtained with voxelisation.

Chapter 9

Comparison with Discrete Data

Furthermore, DASOS allows the user to choose whether the waveform samples or the discrete returns are inserted into the 3D density volume. Each sample or each return has a hit point and an intensity value. So, in both case the space is divided into 3D voxels and the intensity of each return or sample is inserted into the voxel it lies inside.

In general the results of discrete returns contain less information compared to the results from the FW LiDAR, even though the FW LiDAR contain information from about half of the emitted pulses (Section 3). As shown on the 1st example of table 3 the polygon mesh generated from the FW LiDAR contains more details comparing to the one created from the discrete LiDAR. The forest on the top is more detailed, the warehouses in the middle have a clearer shape and the fence on the right lower corner is continuous while in the discrete data it is disconnected and merged with the aliasing.

FW LiDAR polygons, compared to the discrete LiDAR ones, contain more geometry below the outlined surface of the trees. On the one hand this is positive because they include much information about the tree branches but on the other hand the complexity of the objects generated is high. A potential use of the polygon representations is in movie productions: instead of creating a 3D virtual city or forest from scratch, the area of interest can be scanned and then polygonised using our system.

But for efficiency purposes in both animation and rendering, polygonal objects should be closed and their faces should be connected. Hence, in movie productions, polygons generated from the FW LiDAR will require more post-processing in comparison with object generated from the discrete LiDAR.

Example 2 in table 3 shows the differences in the geometry complexity of the discrete and FW polygons using the x-ray shader of Meshlab. The brighter the surface appears the more geometry exists below the top surface. The brightness difference between area 1 and area 2 appears less in the discrete polygon.

Nevertheless, the trees in area 2 are much taller than in area 1, therefore more geometry should have existed in area 2 and sequentially be brighter. But the two areas are only well-distinguished in the FW LiDAR. On average the FW polygon is brighter than the discrete polygon, which implies higher geometry complexity in the FW polygon.

The comparison example 3 is rendered using the Radiance Scaling shader of Meshlab (Vergne et al, 2010). The shader highlights the details of the mesh, making the comparison easier. Not only the FW polygons are more detailed but also holes appear on the discrete polygons. The resolution of the voxels of those examples is 1.7m3 is, the bigger the holes are, while the full-waveform can be polygonised at a resolution of 1m3 without any significant holes. Figure 4 shows an example of rendering the same flightline of examples 3 at the resolution of 1m3 LiDAR data.

The last two examples (4 and 5) compare the side views of small regions. On the one hand the top of the trees are better-shaped in the discrete data. This may occur either because the discrete data contain information from double pulses than the FW data (Section 3) or because the noise threshold of the waveforms is not accurate and the top of the trees appear noisier on the FW LiDAR data. On the other hand more details appear close to the ground on the FW LiDAR data.

*** left during copying :s (and the higher the resolution, using FW)

Chapter 10

Overall Results

Chapter 11

Conclusions

11.1 Contributions

Bibliography

[1] T. Elmqvist, C. Folke, M. Nyström, G. Peterson, J. Bengtsson, B. Walker, and J. Norberg, "Response diversity, ecosystem change, and resilience," *Frontiers in Ecology and the Environment*, vol. 1, no. 9, pp. 488–494, 2003.

[2] D. U. Hooper, F. S. Chapin Iii, J. J. Ewel, A. Hector, P. Inchausti, S. Lavorel, and B. Schmid, "Effects of biodiversity on ecosystem functioning: a consensus of current knowledge," *Ecological monographs*, vol. 75, no. 1, pp. 3–35, 2005.

[3] D. B. Lindenmayer and J. T. Wood, "Long-term patterns in the decay, collapse, and abundance of trees with hollows in the mountain ash (eucalyptus regnans) forests of victoria, southeastern australia," *Canadian Journal of Forest Research*, vol. 40, no. 1, pp. 48–54, 2010.

[4] R. L. Goldingay, "Characteristics of tree hollows used by australian birds and bats," *Wildlife Research*, vol. 36, no. 5, pp. 394–409, 2009.

[5] P. Gibbons and D. Lindenmayer, *Tree Hollows and Wildlife Conservation in Australia*. CSIRO Publishing, 2002.

[6] "Animal pests: Poss."

[7] D. H. DeHayes, P. G. Schaberg, G. J. Hawley, and G. R. Strimbeck, "Acid rain impacts on calcium nutrition and forest health alteration of membrane-associated calcium leads to membrane destabilization and foliar injury in red spruce," *BioScience*, vol. 49, no. 10, pp. 789–800, 1999.

[8] J. Holmgren, "Prediction of tree height, basal area and stem volume in forest stands using airborne laser scanningce," *Scandinavian Journal of Forest Researcht*, vol. 19, no. 6, pp. 543–553, 2004.

[9] S. G. Aracil and R. B. A. Herries, D.L, "Evaluation of an additional lidar metric in forest inventory," *Proceedings of Silvilaser*, 2015.

[10] M. J. Harper, M. A. McCarthy, R. Van Der Ree, and J. C. Fox, "Overcoming bias in ground-based surveys of hollow-bearing trees using double-sampling," *Forest Ecology and Management*, vol. 190, no. 2, pp. 291–300, 2004.

[11] L. Rayner, M. Ellis, and J. E. Taylor, "Double sampling to assess the accuracy of ground-based surveys of tree hollows in eucalypt woodlands," *Forest Ecology and Management*, vol. 36, no. 3, pp. 252–260, 2011.

[12] R. B. Smith, *Introduction to Hyperspectral Imaging*. MicroImages, 2014.

[13] W. Wanger, A. Ullrich, T. Melzer, C. Briese, and K. Kraus, "From single-pulse to ful-waveform airborne laser scanners," *ISPRS Journal of Photogrammetry and Remote Sensing*, vol. 60, pp. 100–112, 2004.

[14] A. Wehr and U. Lohr, "Airborne laser scanning - an introduction and overview," *ISPRS Journal of Photogrammerty and Remote Sensing*, vol. 54, pp. 68–82, 1999.

[15] C. Mallet and F. Bretar, "Full-waveform topographic lidar: State-of-the-art," *ISPRS Journal of Photogrametry and Remote Sensing*, vol. 64, pp. 1–16, 2009.

[16] K. Anderson, S. Hancock, M. Disney, and K. Gaston, "Is waveform worth it? a comparison of lidar approaches for vegetation and landscape characterization," *Remote Sensing in Ecology and Conservation*, 2015.

[17] A. Chauve, C. Mallet, F. Bretar, S. Durrieu, M. Deseilligny, and W. Puech, "Processing full-waveform lidar data: Modelling raw signals," *International Archives of Photogrammetry, Remote Sensing and Spatial Information Sciences*, 2007.

[18] *LAS Specification version 1.3-R1*. Bethesda, Maryland: American Society for Photogrammetry and Remote Sensing, 2010.

[19] M. Warren, *Full Waveform Upgrade*. NERC ARSF wiki, 2012.

[20] M. J. Sumnall, R. A. Hill, and S. A. Hinsley, "Comparison of small-footprint discrete return and full waveform airborne lidar data for estimating multiple forest variables," *Remote Sensing of Environment*, vol. 173, pp. 214–223, 2016.

[21] K. H. R. A. . Z. A. Lehner, H., "Consideration of laser pulse fluctuations and automatic gain control in radiometric calibration of airborne laser scanning data.," *Proceedings of 6th ISPRS Student Consortium and WG VI/5 Summer School*, 2011.

[22] I. Korpela, H. O. Ørka, H. V. Hyyppä, J., and T. Tokola, "Range and agc normalization in airborne discrete-return lidar intensity data for forest canopies," vol. 65, no. 4, pp. 369–379, 2010.

[23] M. Isenburg, *LAStools - efficient tools for LiDAR processing.* rapidlasso.

[24] M. Warren, B. Taylor, M. Grant, and J. D. Shutler, "Data processing of remorely sensed airborne hyperspectral data using the airborne processing library (apl)," *ScienceDirect, Computers and Geosciences*, vol. 64, 2014.

[25] M. Isenburg, "Pulsewaves: An open, vendor-neutral, stand-alone, las-compatible full waveform lidar standard.," 2012.

[26] A. Persson, U. Soderman, J. Topel, and S. Ahlberg, *Visualisation and Analysis of full-waveform airborne laser scanner data.* V/3 Workshop, Laser scanning 2005, 2005.

[27] M. Miltiadou, M. A. Warren, M. Grant, and M. Brown, "Alignment of hyperspectral imagery and full-waveform lidar data for visualisation and classification purposes," *The International Archives of Photogrammetry, Remote Sensing and Spatial Information Sciences*, vol. 40, no. 7, p. 1257, 2015.

[28] W. Wanger, A. Ullrich, V. Ducic, T. Maizer, and N. Studnicka, "Gaussian decompositions and calibration of a novel small-footprint full-waveform digitising airborne laser scanner," *ISPRS Journal of Photogrammetry and Remote Sensing*, vol. 60, pp. 100–112, 2006.

[29] A. Neuenschwander, L. Magruder, and M. Tyler, "Landcover classification of small-footprint full-waveform lidar data," *Jounal of Applied Remote Sensing*, vol. 3, no. 1, pp. 033544–033544.

[30] J. Reitberger, P. Krzystek, and U. Stilla, "Analysis of full waveform LiDAR data for tree species classification," *International Journal of Remote Sensing*, vol. 29, no. 5, pp. 1407–1431, 2008.

[31] L. Cao, N. Coops, L. Innes, J. Dai, and H. Ruan, "Tree species classification in subtropical forests using small-footprint full-waveform lidar data," *International Journal of Applied Earth Observation and Geoinformation*, vol. 49, pp. 39–51, 2016.

[32] M. Miltiadou, M. Grant, M. Brown, M. Warren, and E. Carolan, "Reconstruction of a 3d polygon representation from full-wavefrom lidar data," *RSPSoc Annual Conference 2014, New Sensors for a Changing World*, 2014.

[33] J. F. Blinn, *A Generalization of Algebraic Surface Drawing*, vol. 1. ACM Transactions on Graphics (TOG).

[34] A. Pasko and V. Savchenko, *Blending operations for the functionally based constructive geometry*. 1994.

[35] P. Hanrahan, "Ray tracing algebraic surfaces," *ACM SIGGRAPH Computer Graphics*, vol. 17, no. 3., 1983.

[36] W. E. Lorensen and H. E. Cline, "Marching cubes: A high resolution 3d surface construction algorithm," *ACM Siggraph Computer Graphics*, vol. 21, pp. 163–169, 1987.

[37] M. L. Clark, D. A. Roberts, J. J. Ewel, and D. B. Clark, "Estimation of tropical rain forest aboveground biomas with small-foorprint lidar and hyperspectral sensors," *ScienceDirect, Remote Sensing of Enviroment*, vol. 115.

[38] J. E. Anderson, L. C. Plourde, M. E. Martin, B. H. Braswell, M. L. Smith, R. O. Dubayah, M. A. H. Dubayah, and J. B. Blair, "Integrating waveform lidar with hyperspectral imagery for inventory of a northern temperate forest," *Remote Sensing of Environment*, vol. 112, no. 4, pp. 1856–1870, 2008.

[39] H. Buddenbaum, S. Seeling, and J. Hill, "Fusion of full-waveform lidar and imaging spectroscopy remote sensing data for the characterization of forest stands," *International Journal of Remote Sensing*, vol. 32, no. 13, pp. 4511–4524, 2013.

[40] J. Heinzel and B. Koch, "Investigating multiple data sources for tree species classification in temperate forest and use for single tree delineation," *International Journal of Applied Earth Observation and Geoinformation*, vol. 18, pp. 101–110, 2012.

[41] W. Yao, P. Krzystek, and M. Heurich, "Identifying standing dead trees in forest areas based on 3d single tree detection from full-waveform lidar data," *ISPRS Annals of the Photogrammetry, Remote Sensing and Spatial Information Sciences*, vol. I-7, pp. 359–364, 2012.

[42] P. Polewski, W. Yao, M. Heurich, P. Krzystek, and U. Stilla, "Active learning approach to detecting standing dead trees from als point clouds combined with aerial infrared imagery," *Proceedings of the IEEE Conference on Computer Vision and Pattern Recognition Workshops*, pp. 10–18, 2015.

Chapter 12

Appendices

12.1 Birds and Mammals Catalogue

12.1.0.1 Introduction

12.1.0.2 Australian arboreal Mammals

12.1.0.3 Australian Birds

The Forestry Corporation, Australia, provided a list of bird species that rely on hollows. But species are not limited to that list and more species rely uses hollows for shelters.

The provided list of the birds is divided into three groups:

1. Categorised as threatened species according to the Environement Protection and Biodiversity Conservation Act, 1999

Corella Eastern Rosella Superb Parrot Barking Owl Masked Owl

2. All the above species are included to the Action Plan for Australian Birds, 2000, as well as the following once:

Powerful Owl Sooty Owl

3. The rest:

Kookaburra Sulphur Crested Cockatoo Crimson Rosella Rainbow Lorikeet Musk Lorikeet Little Lorikeet Red-winged Parrot Cockatiel Australian Ringneck (Parrot) Red-rumped Parrot Powerful Owl Sooty Owl Barn Owl White-throated Treecreeper

12.1.0.4 Web-links of Photos

Mammals · Brush-tailed Possum - protected wildlife (Hollow: http://www.cavershamwildlife.com.au/comm brushtail-possum/) (`http://www.rymich.com/girraween/photos/animals/mammals/possums/trichosu`

Birds · Kookaburra (`http://tenrandomfacts.com/blue-winged-kookaburra/`) · Sulphur Crested Cockatoo (`http://aussiegal7.deviantart.com/art/Sulphur-Crested-Cockatoo-08-`

· Corella (http://www.theparrotplace.co.nz/all-about-parrots/long-billed-corella/) · Crimson Rosella (http://25.media.tumblr.com/tumblr_m3mo89c40r1r4t9h1o1_1280.jpg) · Eastern Rosella (http://2.bp.blogspot.com/-pYxw51WjSOY/UB-LEFgd2KI/AAAAAAAAAWg/9z60PUWE6TE/s1600/_GJS6601-as-Smart-Object-1.jpg) · Galah (https://www.pinterest.com/pin/537546905498955709/) · Rainbow Lorikeet (https://www.reddit.com/r/pics/comments/328fvc/a_rainbow_lorikeet_found_in_coastal_regions/) · Musk Lorikeet ((http://www.rymich.com/girraween/photos/animals/birds/medium/glossopsitta_concinna/glossopsitta_concinna_001.jpg) · Little Lorikeet (http://www.pbase.com/sjmurray/psittacidae) · Red-winged Parrot (https://www.pinterest.com/pin/395894623469889727/) · Superb Parrot (http://www.davidkphotography.com/?showimage=637) · Cockatiel (http://up.parsipet.ir/uploads/Cockatiels-for-sale.jpg) · Australian Ringneck (Parrot) (http://ontheroadmagazine.com.au/wp-content/uploads/2015/09/Twenty-eight-parrot-2jpg) · Red-rumped Parrot (http://parrotfacts.net/wp-content/uploads/Red-Rumped-Parrot-on-a-jpg) · Powerful Owl (http://farm1.staticflickr.com/219/495796536_f78dac04c1.jpg) · Sooty Owl (hollow: http://www.mariewinn.com/marieblog/uploaded_images/screech2-738532.jpg) (http://www.owlpages.com/owls/species/images/greater_sooty_owl_richard_jackson-1.jpg) · Barking Owl (http://www.pcpimages.com/Nature-and-Wildlife-Birds/i-7JKSTp5/1/L/owl%20%281%20of%201%29-L.jpg) · Masked Owl (http://www.survival.org.au/images/birds/masked_owl_2_600.jpg) · Barn Owl (Hollow: http://www.barnowltrust.org.uk/wp-content/uploads/Barn_Owl_hollow_tree-wallpaper.jpg) (https://upload.wikimedia.org/wikipedia/commons/c/c6/Tyto_alba_-British_Wildlife_Centre,_Surrey,_England-8a_%281%29.jpg)

· White-throated Treecreeper (http://www.birdlifemelbourne.org.au/bird-lists/47-Treecreepers/White-throated-Treecreeper/White-throated%20Treecreeper%202%20JB.jpg) (hollow: https://geoffpark.files.wordpress.com/2011/09/female-white-throated-trejpg)

Hollow Owl : http://www.mariewinn.com/marieblog/uploaded_images/screech2-738532.jpg